
Segment Any 3D Gaussians

Jiazhong Cen¹, Jiemin Fang², Chen Yang¹,
Lingxi Xie², Xiaopeng Zhang², Wei Shen^{1✉}, Qi Tian²

¹MoE Key Lab of Artificial Intelligence, AI Institute, Shanghai Jiao Tong University

²Huawei Inc.

Abstract

This paper presents SAGA (Segment Any 3D GAussians), a highly efficient 3D promptable segmentation method based on 3D Gaussian Splatting (3D-GS). Given 2D visual prompts as input, SAGA can segment the corresponding 3D target represented by 3D Gaussians within **4 ms**. This is achieved by attaching a scale-gated affinity feature to each 3D Gaussian to endow it a new property towards multi-granularity segmentation. Specifically, a scale-aware contrastive training strategy is proposed for the scale-gated affinity feature learning. It 1) distills the segmentation capability of the Segment Anything Model (SAM) from 2D masks into the affinity features and 2) employs a soft scale gate mechanism to deal with multi-granularity ambiguity in 3D segmentation through adjusting the magnitude of each feature channel according to a specified 3D physical scale. Evaluations demonstrate that SAGA achieves real-time multi-granularity segmentation with quality comparable to state-of-the-art methods. As one of the first methods addressing promptable segmentation in 3D-GS, the simplicity and effectiveness of SAGA pave the way for future advancements in this field. Our code will be released.

1 Introduction

Promptable segmentation has attracted increasing attention and has seen significant advancements, particularly with the development of 2D segmentation foundation models such as the Segment Anything Model (SAM) [24]. However, 3D promptable segmentation remains relatively unexplored due to the scarcity of 3D data and the high cost of annotation. To address these challenges, many studies [7, 10, 53, 23, 11, 35] have proposed to extend SAM’s 2D segmentation capabilities to 3D using radiance fields, achieving notable success.

In this paper, we focus on promptable segmentation in 3D Gaussian Splatting (3D-GS) [21], which represents a significant milestone in radiance fields research due to its superior rendering quality and efficiency compared to its predecessors. We highlight that, in contrast to previous radiance fields, the explicit 3D Gaussian structure can be an ideal carrier for 3D segmentation, as segmentation capabilities can be integrated into 3D-GS as an intrinsic attribute, without necessitating an additional bulky segmentation module.

Accordingly, we propose SAGA (Segment Any 3D GAussians), a 3D promptable segmentation method that integrates the segmentation capabilities of SAM into 3D-GS seamlessly. SAGA takes 2D visual prompts as input and outputs the corresponding 3D target represented by 3D Gaussians. To achieve this purpose, two primary challenges are faced. First, SAGA should figure out an efficient way to endow each 3D Gaussian with the ability of 3D segmentation, so that the high efficiency of 3D-GS can be preserved. Second, as a robust promptable segmentation method, SAGA must

[✉]Corresponding author: wei.shen@sjtu.edu.cn

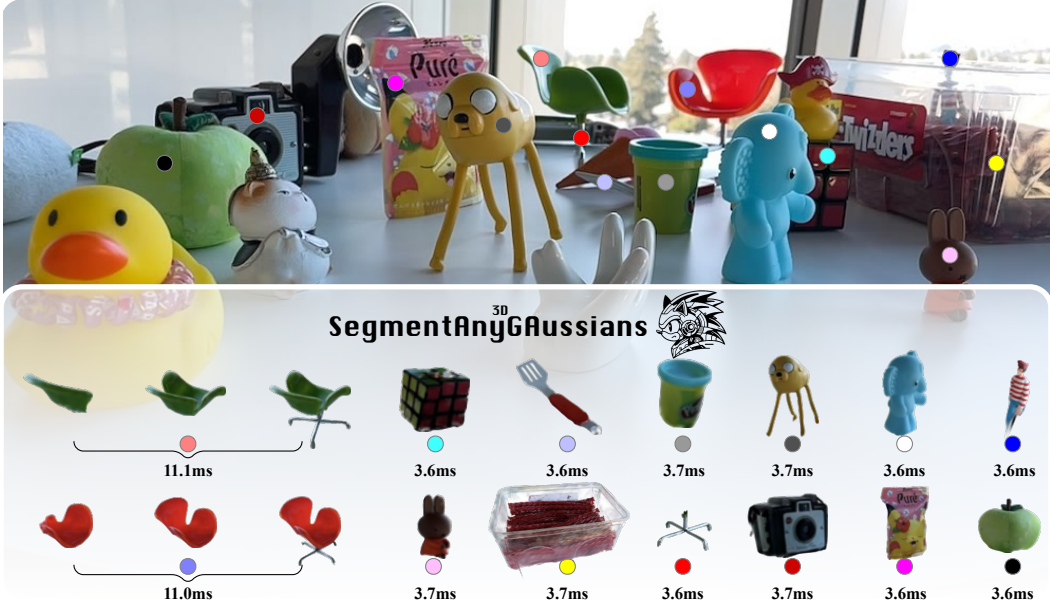


Figure 1: SAGA performs promptable multi-granularity segmentation within **milliseconds**. Prompts are points marked by colors.

effectively address multi-granularity ambiguity, where a single 3D Gaussian may belong to different parts or objects at varying levels of granularity.

To address the two challenges, SAGA respectively introduces two solutions. First, SAGA attaches an affinity feature to each 3D Gaussian in a scene to endow it with a new property towards segmentation. The similarity between two affinity features indicates whether the corresponding 3D Gaussians belong to the same 3D target. Second, inspired by GARField [23], SAGA employs a soft scale gate mechanism to handle multi-granularity ambiguity. Depending on a specified 3D physical scale, the scale gate adjusts the magnitude of each feature channel. This mechanism maps the Gaussian affinity features into different sub-spaces for various scales, thereby preserving the multi-granularity information and meanwhile mitigating the distraction in feature learning brought by multi-granularity ambiguity. More specifically, to realize the two solutions, SAGA proposes a scale-aware contrastive training strategy, which distills the segmentation capability of SAM from 2D masks into scale-gated affinity features. This strategy determines the correlations between each pair of pixels within an image based on given 3D scales. These correlations are then used to supervise the rendered affinity features through a correspondence distillation loss. The correlation information is transmitted to the Gaussian affinity features via backpropagation facilitated by the differentiable rasterization algorithm. After training, SAGA achieves real-time multi-granularity segmentation precisely.

Thanks to the native integration of 3D-GS, SAGA is quite efficient. As illustrated in Figure 1, by taking 2D prompts as input, SAGA can segment each 3D target within **4 ms**, making it the fastest method currently available. Evaluations on existing benchmarks demonstrate that the segmentation quality of SAGA is on par with previous state-of-the-art methods. Furthermore, with well-trained affinity features, SAGA is capable of automatic scene decomposition and open-vocabulary segmentation. We believe the simplicity and effectiveness of SAGA can pave the way for future advancements in promptable segmentation within 3D-GS.

2 Related Work

2D Promptable Segmentation The task of 2D promptable segmentation is proposed by Kirillov *et al.* [24]. The goal of this task is to return segmentation masks given input prompts that specify the segmentation target in an image. To address this problem, they introduce the Segment Anything Model (SAM), a groundbreaking segmentation foundation model. A similar model to SAM is

SEEM [56], which also achieves competitive performance. Prior to these models, the most closely related task to promptable 2D segmentation is interactive image segmentation, which has been explored in numerous studies [4, 16, 17, 44, 9, 45, 31].

3D Segmentation in Radiance Fields Inspired by the success of radiance fields [37, 48, 8, 1, 39, 19, 13, 51, 29, 12], numerous studies have explored 3D segmentation within them. Zhi *et al.* [55] proposed Semantic-NeRF, demonstrating the potential of Neural Radiance Field (NeRF) in semantic propagation and refinement. NVOs [43] introduced an interactive approach to select 3D objects from NeRF by training a lightweight multi-layer perceptron (MLP) using custom-designed 3D features. By using 2D self-supervised models, approaches like N3F [49], DFF [26], and ISRF [15] aim to elevate 2D visual features to 3D by training additional feature fields that can output 2D feature maps, imitating the original 2D features from different views. NeRF-SOS [11] distills the 2D feature similarities into 3D features. There are also some other instance segmentation and semantic segmentation approaches [46, 40, 54, 33, 34, 3, 14, 50] for radiance fields. Combined with CLIP, some approaches [22, 30, 2, 41] proposed to conduct open-vocabulary 3D segmentation in radiance fields. With the popularity of SAM, a stream of studies [23, 53, 52, 7] proposed lifting the segmentation ability of SAM to 3D with radiance fields. SA3D [7] adopts an iterative pipeline to refine the 3D mask grids with SAM. GaussianGrouping [52] uses video tracking technology to align the inconsistent 2D masks extracted by SAM across different views and assigns labels to 3D Gaussians in a 3D-GS model with the aligned masks. OmniSeg3D [53] employs a hierarchical contrastive learning method to automatically learn hierarchical segmentation from multi-view 2D masks extracted by SAM.

The approach most closely related to SAGA is GARField [23], which uses 3D physical scale as a condition for 3D feature fields to address the multi-granularity ambiguity in 3D segmentation. This concept inspires the scale gate mechanism of SAGA. However, GARField relies on an implicit feature field to output features in 3D space. For each segmentation at different scales, GARField must repeatedly query the scale-conditioned field, significantly hindering segmentation efficiency. In contrast, the scale-gate mechanism of SAGA can be applied to 3D-GS without introducing additional neural networks, thereby enhancing SAGA’s efficiency.

3 Method

In this section, we first give a brief review of 3D Gaussian Splatting (3D-GS) [21] and the scale-conditioned 3D features [22, 23]. Then we introduce the overall pipeline of SAGA, followed by explanation of the scale-gated Gaussian affinity features and the scale-aware contrastive learning.

3.1 Preliminary

3D Gaussian Splatting (3D-GS) Given a training dataset \mathcal{I} of multi-view 2D images with camera poses, 3D-GS learns a set of 3D colored Gaussians $\mathcal{G} = \{\mathbf{g}_1, \mathbf{g}_2, \dots, \mathbf{g}_N\}$, where N denotes the number of 3D Gaussians in the scene. The mean of a Gaussian represents its position and the covariance indicates its scale. Accordingly, 3D-GS proposes a novel differentiable rasterization technology for efficient training and rendering. Given a specific camera pose, 3D-GS projects the 3D Gaussians to 2D and computes the color $\mathbf{C}(\mathbf{p})$ of a pixel \mathbf{p} by blending a set of ordered Gaussians $\mathcal{G}_{\mathbf{p}}$ overlapping the pixel. Let $\mathbf{g}_i^{\mathbf{p}}$ denote the i -th Gaussian in $\mathcal{G}_{\mathbf{p}}$, this process is formulated as:

$$\mathbf{C}(\mathbf{p}) = \sum_{i=1}^{|\mathcal{G}_{\mathbf{p}}|} \mathbf{c}_{\mathbf{g}_i^{\mathbf{p}}} \alpha_{\mathbf{g}_i^{\mathbf{p}}} \prod_{j=1}^{i-1} (1 - \alpha_{\mathbf{g}_j^{\mathbf{p}}}), \quad (1)$$

where $\mathbf{c}_{\mathbf{g}_i^{\mathbf{p}}}$ is the color of $\mathbf{g}_i^{\mathbf{p}}$ and $\alpha_{\mathbf{g}_i^{\mathbf{p}}}$ is given by evaluating the corresponding 2D Gaussian with covariance Σ multiplied with a learned per-Gaussian opacity.

Scale-Conditioned 3D Feature LERF [22] first proposes the concept of a scale-conditioned feature field for learning from global image embeddings obtained from CLIP. GARField [23] then introduces it into the area of radiance field segmentation to tackle the multi-granularity ambiguity. To compute the 3D mask scale $s_{\mathbf{M}}$ of a 2D mask \mathbf{M} , GARField projects \mathbf{M} into 3D space with the camera intrinsic parameters and depth information predicted by a pre-trained radiance field. Let \mathcal{P} denote

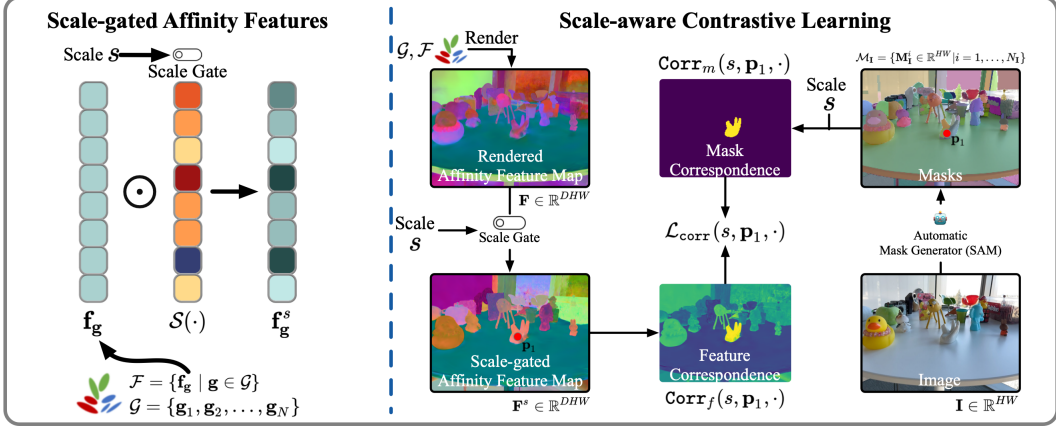


Figure 2: The architecture of SAGA. *Left*: SAGA attaches a Gaussian affinity feature to each 3D Gaussian. The magnitude of different affinity feature channels are adjusted by a soft scale gate to handle multi-granularity ambiguity. *Right*: SAGA distills segmentation ability of SAM into affinity features attached to 3D Gaussians in the 3D-GS model through scale-aware contrastive learning.

the obtained point cloud, $\mathcal{X}(\mathcal{P})$, $\mathcal{Y}(\mathcal{P})$, $\mathcal{Z}(\mathcal{P})$ denote the set of 3D coordinate components of \mathcal{P} , the mask scale s_M is:

$$s_M = 2\sqrt{\text{std}(\mathcal{X}(\mathcal{P}))^2 + \text{std}(\mathcal{Y}(\mathcal{P}))^2 + \text{std}(\mathcal{Z}(\mathcal{P}))^2}, \quad (2)$$

where $\text{std}(\cdot)$ denotes the standard variation of a set of scalars. Since these scales are computed in 3D space, they are generally consistent across different views. SAGA uses the 3D scales for multi-granularity segmentation but realizes it in a more efficient way.

3.2 Overall Pipeline

The main components of SAGA are shown in Figure 2. Given a pre-trained 3D-GS model \mathcal{G} , SAGA attaches a Gaussian affinity feature $\mathbf{f}_g \in \mathbb{R}^D$ for each 3D Gaussian \mathbf{g} in \mathcal{G} . D denotes the feature dimension. To handle the inherent multi-granularity ambiguity of 3D promptable segmentation, SAGA employs a soft scale gate mechanism to project these features into different scale-gated feature subspaces for various scales s .

To train the affinity features, SAGA extracts a set of multi-granularity masks $\mathcal{M}_I = \{\mathbf{M}_i^i \in \{0, 1\}^{HW} \mid i = 1, \dots, N_I\}$ for each image \mathbf{I} in the training set \mathcal{I} with SAM. H, W denotes the height and width of \mathbf{I} respectively. N_I denotes the number of extracted masks. For each mask \mathbf{M}_i^i , its corresponding 3D physical scale $s_{M_i^i}$ is calculated using the depth predicted by \mathcal{G} with the camera pose, as shown in Equation (2). Subsequently, SAGA employs a scale-aware contrastive learning strategy (Section 3.3.2) to distill the multi-granularity segmentation ability embedded in multi-view 2D masks into the scale-gated affinity features. After training, at given scales, the affinity feature similarities between two Gaussians indicate whether they belong to the same 3D target.

During inference (Section 3.4), given a specific viewpoint, SAGA takes 2D visual prompts (with scales) as input and converts them to corresponding 3D scale-gated query features, which are then used to segment the 3D target by evaluating feature similarities with scale-gated 3D affinity features. Additionally, with the well-trained affinity features, 3D scene decomposition can be achieved through straightforward clustering. Furthermore, by integrating with CLIP, SAGA can perform open-vocabulary segmentation (Section A.3) without the need for additional language fields.

3.3 Gaussian Affinity Feature Learning

At the core of SAGA is the Gaussian affinity features $\mathcal{F} = \{\mathbf{f}_g \mid \mathbf{g} \in \mathcal{G}\}$, which are learned from the multi-view 2D masks extracted by SAM. To tackle the inherent multi-granularity ambiguity in promptable segmentation, inspired by GARfield [23], we introduce a scale gate mechanism to split the feature space into different sub-spaces for various 3D physical scales. Then, a 3D Gaussian

can belong to different segmentation targets at different granularities without conflict. To get these scale-gated features, we adopt a scale-aware contrastive learning strategy.

3.3.1 Scale-Gated Affinity Features

Given a Gaussian affinity feature \mathbf{f}_g and a specific scale s , SAGA adopts a scale gate to adapt the magnitude of different feature channels accordingly. The scale gate is defined as a mapping $\mathcal{S} : [0, 1] \rightarrow [0, 1]^D$, which projects a scale scalar $s \in [0, 1]$ to its corresponding soft gate vector $\mathcal{S}(s)$. To maximize segmentation efficiency, the scale gate adopts an extremely streamlined design, which is composed with a single linear layer followed by a sigmoid function. At the scale of s the scale-gated affinity feature is:

$$\mathbf{f}_g^s = \mathcal{S}(s) \odot \mathbf{f}_g, \quad (3)$$

where \odot denotes the Hadamard product. Thanks to the simplicity of the scale gate mechanism, the time overhead caused by scale changing is negligible.

Since all Gaussian affinity features share a common scale gate at scale s , during training, we can first render the affinity features to 2D and then apply the scale gate to the 2D rendered features, *i.e.*,

$$\mathbf{F}(\mathbf{p}) = \sum_{i=1}^{|\mathcal{G}_p|} \mathbf{f}_{g_i^p} \alpha_{g_i^p} \prod_{j=1}^{i-1} (1 - \alpha_{g_j^p}), \quad (4)$$

$$\mathbf{F}^s(\mathbf{p}) = \mathcal{S}(s) \odot \mathbf{F}(\mathbf{p}). \quad (5)$$

During inference, the scale gate is directly applied to the 3D Gaussian affinity features for conducting 3D segmentation.

Local Feature Smoothing In practice, we find that there are many noisy Gaussians in the 3D space that exhibit unexpectedly high feature similarities with the segmentation target. This may occur for various reasons, such as insufficient training due to small weights in rasterization or incorrect geometry structure learned by 3D-GS. To tackle this problem, we adopt the spatial locality prior of 3D Gaussians. During training, SAGA uses the smoothed affinity feature of a Gaussian \mathbf{g} to replace its original feature \mathbf{f}_g , *i.e.*, $\mathbf{f}_g \leftarrow \frac{1}{K} \sum_{g' \in \text{KNN}(\mathbf{g})} \mathbf{f}_{g'}$. $\text{KNN}(\mathbf{g})$ denotes K -nearest neighbors of \mathbf{g} .

After training, the affinity feature for each 3D Gaussian is saved as its smoothed feature. Consequently, there is no need to perform KNN during inference, thus avoiding additional computational overhead.

3.3.2 Scale-Aware Contrastive Learning

To train the scale-gated affinity features, for an image \mathbf{I} of a specific view, we first convert the automatically extracted 2D masks \mathcal{M}_I to scale-aware supervision signal.

Scale-Aware Pixel Identity Vector We assign a scale-aware pixel identity vector $\mathbf{V}(s, \mathbf{p}) \in \{0, 1\}^{N_I}$ to each pixel \mathbf{p} in an image \mathbf{I} . The identity vectors reflect the 2D masks that a pixel belong to at specific scales. Intuitively, if two pixels $\mathbf{p}_1, \mathbf{p}_2$ share at least a same mask at a given scale (*i.e.*, $\mathbf{V}(s, \mathbf{p}_1) \cdot \mathbf{V}(s, \mathbf{p}_2) > 0$), they should have similar features at scale s .

To obtain $\mathbf{V}(s, \mathbf{p})$, we first sort the mask set \mathcal{M}_I in descending order according to their mask scales and get an ordered mask list $\mathcal{O}_I = (\mathbf{M}_I^{(1)}, \dots, \mathbf{M}_I^{(N_I)})$, where $s_{\mathbf{M}_I^{(1)}} > \dots > s_{\mathbf{M}_I^{(N_I)}}$. Then, for a pixel \mathbf{p} , when $s_{\mathbf{M}_I^{(i)}} < s$, the i -th entry of $\mathbf{V}(s, \mathbf{p})$ is set to $\mathbf{M}_I^{(i)}(\mathbf{p})$. When $s_{\mathbf{M}_I^{(i)}} \geq s$, the i -th entry of $\mathbf{V}(s, \mathbf{p})$ equals to 1 only if $\mathbf{M}_I^{(i)}(\mathbf{p}) = 1$ and all smaller masks in $\{\mathbf{M}_I^{(j)} \mid s \leq \mathbf{M}_I^{(j)} < s_{\mathbf{M}_I^{(i)}}\}$ equals to 0 at pixel \mathbf{p} . Formally, we have:

$$\mathbf{V}^i(s, \mathbf{p}) = \begin{cases} \mathbf{M}_I^{(i)}(\mathbf{p}) & \text{if } s_{\mathbf{M}_I^{(i)}} < s \text{ or } \left(\forall \mathbf{M} \in \{\mathbf{M}_I^{(j)} \mid s \leq \mathbf{M}_I^{(j)} < s_{\mathbf{M}_I^{(i)}}\}, \mathbf{M}(\mathbf{p}) = 0 \right) \\ 0 & \text{otherwise} \end{cases} \quad (6)$$

This assignment of pixel identity vectors is based on the assumption that if a pixel belongs to a specific mask at a given scale, it will continue to belong to that mask at larger scales.

Loss Function We adapt the correspondence distillation loss proposed by Hamilton *et al.* [18] for training the scale-gated Gaussian affinity features. Concretely, for two pixels $\mathbf{p}_1, \mathbf{p}_2$ at a given scale s , their mask correspondence is given by:

$$\text{Corr}_m(s, \mathbf{p}_1, \mathbf{p}_2) = \mathbb{1}(\mathbf{V}(s, \mathbf{p}_1) \cdot \mathbf{V}(s, \mathbf{p}_2)), \quad (7)$$

where $\mathbb{1}(\cdot)$ is the indicator function, which is equal to 1 when the input greater than 0 and equal to 0 when the input is 0. The feature correspondence between two pixels is defined as the cosine similarity between their scale-gated features:

$$\text{Corr}_f(s, \mathbf{p}_1, \mathbf{p}_2) = \langle \mathbf{F}^s(\mathbf{p}_1), \mathbf{F}^s(\mathbf{p}_2) \rangle. \quad (8)$$

The correspondence distillation loss $\mathcal{L}_{\text{corr}}(\mathbf{p}_1, \mathbf{p}_2)$ between two pixels is given by¹:

$$\mathcal{L}_{\text{corr}}(s, \mathbf{p}_1, \mathbf{p}_2) = (1 - 2 \text{Corr}_m(s, \mathbf{p}_1, \mathbf{p}_2)) \max(\text{Corr}_f(s, \mathbf{p}_1, \mathbf{p}_2), 0). \quad (9)$$

Feature Norm Regularization During training, the 2D features are obtained by rendering with 3D affinity features. This indicates a misalignment between 2D and 3D features. As revealed in Equation (4), a 2D feature is a linear combination of multiple 3D features, each with distinct directions. In such situations, SAGA may show good segmentation ability on the rendered feature map but perform poorly in 3D space. This motivates us to introduce a feature norm regularization. Concretely, during rendering the 2D feature map, the 3D features are first normalized as unit vectors, *i.e.*,

$$\mathbf{F}(\mathbf{p}) = \sum_{i=1}^{|\mathcal{G}_{\mathbf{p}}|} \frac{\mathbf{f}_{\mathbf{g}_i^{\mathbf{p}}}}{\|\mathbf{f}_{\mathbf{g}_i^{\mathbf{p}}}\|_2} \alpha_{\mathbf{g}_i^{\mathbf{p}}} \prod_{j=1}^{i-1} (1 - \alpha_{\mathbf{g}_j^{\mathbf{p}}}). \quad (10)$$

Accordingly, $\|\mathbf{F}(\mathbf{p})\|_2$ ranges in $[0, 1]$. When 3D features along a ray are perfectly aligned, $\|\mathbf{F}(\mathbf{p})\|_2 = 1$. Thus, we impose a regularization on the rendered feature norm:

$$\mathcal{L}_{\text{norm}}(\mathbf{p}) = 1 - \|\mathbf{F}(\mathbf{p})\|_2 \quad (11)$$

With the feature norm regularization term, for an iteration of training, the loss of SAGA is defined as:

$$\mathcal{L} = \sum_{(\mathbf{p}_1, \mathbf{p}_2) \in \delta(\mathbf{I}) \times \delta(\mathbf{I})} \mathcal{L}_{\text{corr}}(\mathbf{p}_1, \mathbf{p}_2) + \frac{1}{HW} \sum_{\mathbf{p} \in \delta(\mathbf{I})} \mathcal{L}_{\text{norm}}(\mathbf{p}), \quad (12)$$

where $\delta(\mathbf{I})$ denotes the set of pixels within the image \mathbf{I} .

3.3.3 Additional Training Strategy

During the training of SAGA, an unavoidable issue is the data imbalance, which is reflected in three aspects: 1) Most pixel pairs keep to be positive or negative regardless of scale variations, making the learned feature insensitive to scales; 2) The majority of pixel pairs shows negative correspondence, resulting in feature collapse; 3) Large targets that occupy more pixels in images have more effect on the optimization, leading to bad performance of segmenting small targets. We tackle this problem by resampling the sampled pixel-pairs and re-weighting the loss function for different samples. Please refer to Section A.1 for detailed explanation.

3.4 Inference

With well-trained Gaussian affinity features, SAGA can conduct various segmentation tasks in the 3D space. For promptable segmentation, SAGA takes **2D point prompts** at specific view and the scale as input. Then, SAGA segments the 3D target by matching scale-gated 3D Gaussian affinity features with the 2D query features selected from the rendered feature map according to prompt points. For automatic scene decomposing, SAGA employs HDBSCAN to cluster the affinity features directly in the 3D space². Additionally, we design a vote-based segmentation mechanism to integrate SAGA with CLIP [42] for conducting open vocabulary segmentation (see Section A.3).

¹The feature correspondence is clipped at 0 to stabilize training. Please refer to [18] for more details.

²For efficiency, SAGA uniformly selects 1% of the Gaussians from the 3D-GS model for clustering.

4 Experiments

In this section, we demonstrate the effectiveness of SAGA both quantitatively and qualitatively. For implementation details and specific experiment settings, please refer to Section A.2.

4.1 Datasets

For promptable segmentation experiments, we utilize two datasets: Neural Volumetric Object Selection (NVOS)[43] and SPIn-NeRF[38]. The former is derived from the LLFF dataset [36] and the latter is a combination of subsets of data from established NeRF-related datasets [36, 37, 28, 25, 13]. For open-vocabulary segmentation experiments, we adopt the 3D-OVS dataset [30]. For qualitative analysis, we employ various datasets including LLFF [36], MIP-360 [1], Tanks&Temple [25], and Replica [47]. These datasets encompass indoor and outdoor scenes, forward-facing and 360-degree scenes, as well as synthetic and real scenes.

4.2 Quantitative Results

4.2.1 Promptable Segmentation

NVOS Dataset As shown in Table 1, SAGA outperforms previous segmentation approaches for both 3D-GS and other radiance fields, *i.e.*, +0.4 mIoU over the previous SOTA SA3D-GS and +0.9 mIoU over the OmniSeg3D.

SPIn-NeRF Dataset Results on the SPIn-NeRF dataset can be found in Table 2. SA3D performs on par with the previous SOTA OmniSeg3D. The minor performance degradation is attributed to sub-optimal geometry learned by 3D-GS. Specifically, in the “fork” scene, which features a metal fork on a table, the segmentation target is simple (*i.e.*, the fork). However, 3D-GS models the reflection effects of the fork with numerous outlier Gaussians that are not aligned with the exact geometry. Excluding these Gaussians results in empty holes in the segmentation mask for certain views, while including them introduces noise in other views. Nevertheless, we believe the segmentation accuracy of SAGA can meet most requirements.

Table 1: Results on NVOS dataset.

Method	mIoU (%)	mAcc (%)
NVOS [43]	70.1	92.0
ISRF [15]	83.8	96.4
SA3D [7]	90.3	98.2
OmniSeg3D [53]	91.7	98.4
SA3D-GS [6]	92.2	98.5
SAGA (ours)	92.6	98.6

Table 2: Results on SPIn-NeRF dataset.

Method	mIoU (%)	mAcc (%)
MVSeg [38]	90.9	98.9
SA3D [7]	92.4	98.9
OmniSeg3D [53]	94.3	99.3
SA-GS [20]	89.9	98.7
SA3D-GS [6]	93.2	99.1
SAGA (ours)	93.4	99.2

4.2.2 Open-Vocabulary Semantic Segmentation

To conduct open-vocabulary semantic segmentation, we follow the setting of 3D-OVS where all categories are input to CLIP to obtain their textual features. These features are then used to vote for all clusters as introduced in Section 3.4. For each cluster, the category with the highest score is assigned as its label. As shown in Table 3, SAGA demonstrates superior results across all scenes in the 3D-OVS dataset. However, we acknowledge that this result does not imply that SAGA consistently outperforms previous open-vocabulary radiance field segmentation methods. Please refer to Section A.3 for a detailed discussion on the limitations of SAGA in open-vocabulary segmentation.

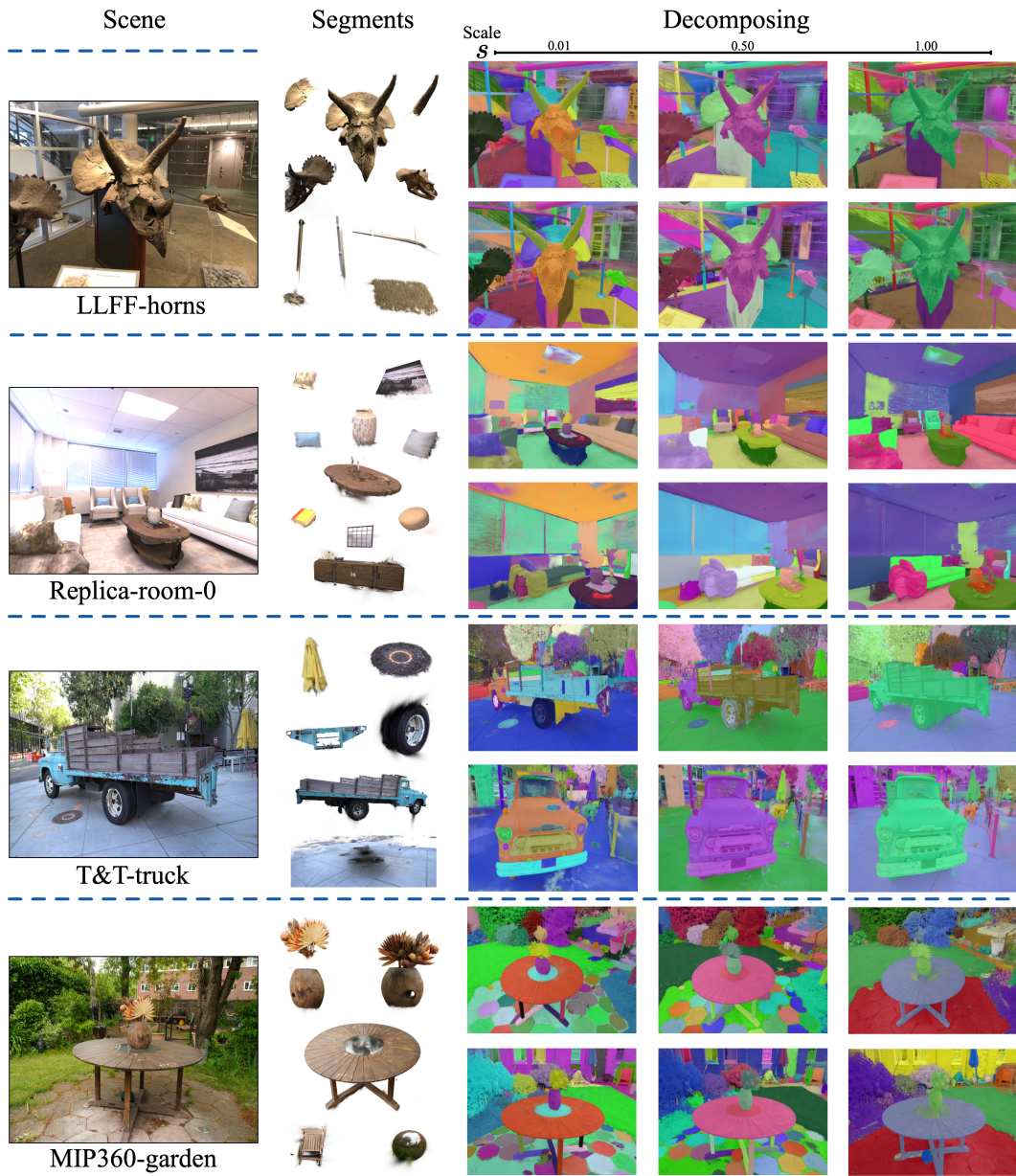


Figure 3: Qualitative results of SAGA across different scenes. We provide both the targets segmented via 2D point prompts and the “segment everything” results.

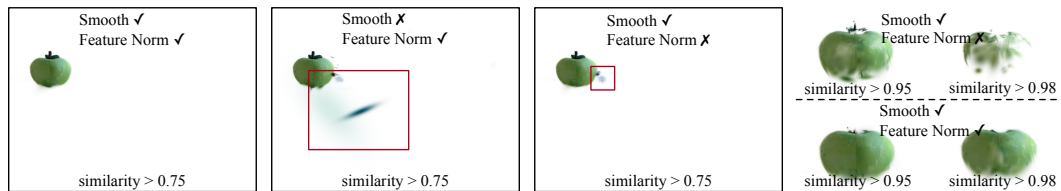


Figure 4: Ablation study on effects of local feature smoothing (Smooth) and feature norm regularization (Feature Norm). Outliers are primarily eliminated through local feature smoothing. Feature norm regularization helps features of inner Gaussians align better with those of the surface Gaussians.

Table 3: Open vocabulary segmentation results on 3D-OVS dataset (mIoU).

Method	bed	bench	room	sofa	lawn	mean
LERF [22]	73.5	53.2	46.6	27.0	73.7	54.8
3D-OVS [30]	89.5	89.3	92.8	74.0	88.2	86.8
LangSplat [41]	92.5	94.2	94.1	90.0	96.1	93.4
N2F2 [41]	93.8	92.6	93.5	92.1	96.3	93.9
SAGA (ours)	97.4	95.4	96.8	93.5	96.6	96.0

4.2.3 Time Consumption Analysis

In Table 4, we reveal the time consumption of SAGA and compare it with existing promptable segmentation methods in radiance fields. ISRF trains a feature field by mimicking the 2D multi-view visual features extracted by DINO [5], thus enjoys faster convergence speed. However, this approach results in less accurate segmentation, necessitating extensive post-processing. SA3D and SA-GS employ an iterative mask refinement pipeline, which eliminates the need for training but incurs significant inference time consumption. Compared to methods that distill segmentation capabilities from SAM masks, such as OmniSeg3D and GARField, SAGA demonstrates much faster inference speed and comparable training speed.

Table 4: Time consumption comparison.

Method	Training	Inference
SA3D [7]	-	45 s
SA-GS [20]	-	15 s
ISRF [15]	2.5 mins	3.3 s
OmniSeg3D [53]	15~40 mins	50~100 ms
GARField [23]	20~60 mins	30~70 ms
SAGA (ours)	10~40 mins	2~5 ms

4.3 Qualitative Results

As shown in Figure 3, SAGA can achieve fine-grained segmentation at different scales in various types of scenes. The learned Gaussian affinity features are compact enough for scene decomposition through simple clustering across the entire 3D-GS model. Note that there are some needle-like burrs on the edges of the segmented targets. This artifact is due to the nature of 3D-GS, which aims to fit multi-view RGB color given camera poses without object awareness. For more visualization results, please refer to our appendix.

4.4 Ablation Study

Local Feature Smoothing & Feature Norm Regularization Both local feature smoothing and feature norm regularization impose constraints on the Gaussian affinity features. We present visualization results to illustrate their roles intuitively.

As shown in Figure 4, when segmenting a 3D object with a cosine similarity threshold of 0.75, SAGA without the feature smoothing mechanism shows many false positives. This indicates that outliers are primarily eliminated by the feature smoothing operation.

Unlike local feature smoothing, feature norm regularization primarily impacts the Gaussians within objects. When raising the similarity score threshold to 0.95, the apple segmented by SAGA with feature norm regularization remains intact, while the one without it quickly becomes translucent. This phenomenon supports our assumption that 3D features are not perfectly aligned with 2D features, as introduced in Section 3.3.2. Imposing feature norm regularization helps align the affinity features of 3D Gaussians by pulling the features along a ray in the same direction.

5 Limitation

SAGA learns the affinity features from multi-view 2D masks extracted by SAM. This makes SAGA hardly segment objects that are not appeared in these masks. Enhancing the generalization ability of SAGA to unrecognized targets during the automatic extraction stage is a promising direction.

6 Conclusion

In this paper, we propose SAGA, a 3D promptable segmentation method for 3D Gaussian Splatting (3D-GS). SAGA injects the segmentation capability of SAM into Gaussian affinity features for all 3D Gaussians in the 3D-GS model, endowing them with a new property towards segmentation. To simultaneously preserve the multi-granularity segmentation ability of SAM and the efficiency of 3D-GS, SAGA introduces a lightweight scale-gate mechanism, which adapts the affinity features according to different 3D physical scales with minimal computation overhead. After training, SAGA can achieve fine-grained 3D segmentation within milliseconds. Comprehensive experiments are conducted to demonstrate the effectiveness of SAGA. As one of the first methods addressing promptable segmentation in 3D-GS, the simplicity and effectiveness of SAGA pave the way for future advancements in this field.

References

- [1] Jonathan T. Barron, Ben Mildenhall, Dor Verbin, Pratul P. Srinivasan, and Peter Hedman. Mip-nerf 360: Unbounded anti-aliased neural radiance fields. In *CVPR*, 2022.
- [2] Yash Bhalgat, Iro Laina, João F. Henriques, Andrew Zisserman, and Andrea Vedaldi. N2f2: Hierarchical scene understanding with nested neural feature fields. *arXiv preprint arXiv:2403.10997*, 2024.
- [3] Wang Bing, Lu Chen, and Bo Yang. Dm-nerf: 3d scene geometry decomposition and manipulation from 2d images. In *ICLR*, 2023.
- [4] Yuri Y Boykov and M-P Jolly. Interactive graph cuts for optimal boundary & region segmentation of objects in nd images. In *ICCV*, 2001.
- [5] Mathilde Caron, Hugo Touvron, Ishan Misra, Hervé Jégou, Julien Mairal, Piotr Bojanowski, and Armand Joulin. Emerging properties in self-supervised vision transformers. In *ICCV*, 2021.
- [6] Jiazhong Cen, Jiemin Fang, Zanwei Zhou, Chen Yang, Lingxi Xie, Xiaopeng Zhang, Wei Shen, and Qi Tian. Segment anything in 3d with radiance fields. *arXiv preprint arXiv:2304.12308*, 2024.
- [7] Jiazhong Cen, Zanwei Zhou, Jiemin Fang, Chen Yang, Wei Shen, Lingxi Xie, Dongsheng Jiang, Xiaopeng Zhang, and Qi Tian. Segment anything in 3d with nerfs. In *NeurIPS*, 2023.
- [8] Anpei Chen, Zexiang Xu, Andreas Geiger, Jingyi Yu, and Hao Su. Tensorf: Tensorial radiance fields. In *ECCV*, 2022.
- [9] Xi Chen, Zhiyan Zhao, Yilei Zhang, Manni Duan, Donglian Qi, and Hengshuang Zhao. Focalclick: Towards practical interactive image segmentation. In *CVPR*, 2022.
- [10] Xiaokang Chen, Jiayang Tang, Diwen Wan, Jingbo Wang, and Gang Zeng. Interactive segment anything nerf with feature imitation. *arXiv preprint arXiv:2305.16233*, 2023.
- [11] Zhiwen Fan, Peihao Wang, Yifan Jiang, Xinyu Gong, Dejie Xu, and Zhangyang Wang. Nerf-sos: Any-view self-supervised object segmentation on complex scenes. In *ICLR*, 2023.
- [12] Jiemin Fang, Taoran Yi, Xinggang Wang, Lingxi Xie, Xiaopeng Zhang, Wenyu Liu, Matthias Nießner, and Qi Tian. Fast dynamic radiance fields with time-aware neural voxels. In *SIG-GRAPH Asia 2022 Conference Papers*, 2022.
- [13] Sara Fridovich-Keil, Alex Yu, Matthew Tancik, Qinhong Chen, Benjamin Recht, and Angjoo Kanazawa. Plenoxels: Radiance fields without neural networks. In *CVPR*, 2022.
- [14] Xiao Fu, Shangzhan Zhang, Tianrun Chen, Yichong Lu, Lanyun Zhu, Xiaowei Zhou, Andreas Geiger, and Yiyi Liao. Panoptic nerf: 3d-to-2d label transfer for panoptic urban scene segmentation. In *3DV*, 2022.
- [15] Rahul Goel, Dhawal Sirikonda, Saurabh Saini, and PJ Narayanan. Interactive segmentation of radiance fields. In *CVPR*, 2023.
- [16] Leo Grady. Random walks for image segmentation. *IEEE Trans. Pattern Anal. Mach. Intell.*, 2006.
- [17] Varun Gulshan, Carsten Rother, Antonio Criminisi, Andrew Blake, and Andrew Zisserman. Geodesic star convexity for interactive image segmentation. In *CVPR*, 2010.

- [18] Mark Hamilton, Zhoutong Zhang, Bharath Hariharan, Noah Snavely, and William T. Freeman. Unsupervised semantic segmentation by distilling feature correspondences. In *ICLR*, 2022.
- [19] Peter Hedman, Pratul P. Srinivasan, Ben Mildenhall, Christian Reiser, Jonathan T. Barron, and Paul Debevec. Baking neural radiance fields for real-time view synthesis. *IEEE TPAMI*, 2024.
- [20] Xu Hu, Yuxi Wang, Lue Fan, Junsong Fan, Junran Peng, Zhen Lei, Qing Li, and Zhaoxiang Zhang. Segment anything in 3d gaussians. *arXiv preprint arXiv:2401.17857*, 2024.
- [21] Bernhard Kerbl, Georgios Kopanas, Thomas Leimkühler, and George Drettakis. 3d gaussian splatting for real-time radiance field rendering. *ACM TOG*, 2023.
- [22] Justin Kerr, Chung Min Kim, Ken Goldberg, Angjoo Kanazawa, and Matthew Tancik. Lerp: Language embedded radiance fields. In *ICCV*, 2023.
- [23] Chung Min* Kim, Mingxuan* Wu, Justin* Kerr, Matthew Tancik, Ken Goldberg, and Angjoo Kanazawa. Garfield: Group anything with radiance fields. In *CVPR*, 2024.
- [24] Alexander Kirillov, Eric Mintun, Nikhila Ravi, Hanzi Mao, Chloe Rolland, Laura Gustafson, Tete Xiao, Spencer Whitehead, Alexander C Berg, Wan-Yen Lo, et al. Segment anything. In *ICCV*, 2023.
- [25] Arno Knapitsch, Jaesik Park, Qian-Yi Zhou, and Vladlen Koltun. Tanks and temples: Benchmarking large-scale scene reconstruction. *ACM TOG*, 2017.
- [26] Sosuke Kobayashi, Eiichi Matsumoto, and Vincent Sitzmann. Decomposing nerf for editing via feature field distillation. In *NeurIPS*, 2022.
- [27] Guibiao Liao, Jiankun Li, Zhenyu Bao, Xiaoqing Ye, Jingdong Wang, Qing Li, and Kanglin Liu. Clip-gs: Clip-informed gaussian splatting for real-time and view-consistent 3d semantic understanding. *arXiv preprint arXiv:2404.14249*, 2024.
- [28] Yen-Chen Lin, Pete Florence, Jonathan T. Barron, Tsung-Yi Lin, Alberto Rodriguez, and Phillip Isola. Nerf-supervision: Learning dense object descriptors from neural radiance fields. In *ICRA*, 2022.
- [29] David B. Lindell, Julien N. P. Martel, and Gordon Wetzstein. Autoint: Automatic integration for fast neural volume rendering. In *CVPR*, 2021.
- [30] Kunhao Liu, Fangneng Zhan, Jiahui Zhang, MUYU XU, Yingchen Yu, Abdulmoteleb El Saddik, Christian Theobalt, Eric Xing, and Shijian Lu. Weakly supervised 3d open-vocabulary segmentation. In *NeurIPS*, 2023.
- [31] Qin Liu, Zhenlin Xu, Gedas Bertasius, and Marc Niethammer. Simpleclick: Interactive image segmentation with simple vision transformers. In *ICCV*, 2023.
- [32] Shilong Liu, Zhaoyang Zeng, Tianhe Ren, Feng Li, Hao Zhang, Jie Yang, Chunyuan Li, Jianwei Yang, Hang Su, Jun Zhu, et al. Grounding dino: Marrying dino with grounded pre-training for open-set object detection. *arXiv preprint arXiv:2303.05499*, 2023.
- [33] Xinhang Liu, Jiaben Chen, Huai Yu, Yu-Wing Tai, and Chi-Keung Tang. Unsupervised multi-view object segmentation using radiance field propagation. In *NeurIPS*, 2022.
- [34] Yichen Liu, Benran Hu, Junkai Huang, Yu-Wing Tai, and Chi-Keung Tang. Instance neural radiance field. In *ICCV*, 2023.
- [35] Yichen Liu, Benran Hu, Chi-Keung Tang, and Yu-Wing Tai. Sanerf-hq: Segment anything for nerf in high quality. *arXiv preprint arXiv:2312.01531*, 2023.
- [36] Ben Mildenhall, Pratul P. Srinivasan, Rodrigo Ortiz Cayon, Nima Khademi Kalantari, Ravi Ramamoorthi, Ren Ng, and Abhishek Kar. Local light field fusion: practical view synthesis with prescriptive sampling guidelines. *ACM TOG*, 2019.
- [37] Ben Mildenhall, Pratul P. Srinivasan, Matthew Tancik, Jonathan T. Barron, Ravi Ramamoorthi, and Ren Ng. Nerf: Representing scenes as neural radiance fields for view synthesis. In *ECCV*, 2020.
- [38] Ashkan Mirzaei, Tristan Aumentado-Armstrong, Konstantinos G. Derpanis, Jonathan Kelly, Marcus A. Brubaker, Igor Gilitschenski, and Alex Levinshtein. SPIn-NeRF: Multiview segmentation and perceptual inpainting with neural radiance fields. In *CVPR*, 2023.
- [39] Thomas Müller, Alex Evans, Christoph Schied, and Alexander Keller. Instant neural graphics primitives with a multiresolution hash encoding. *ACM TOG*, 2022.

- [40] Michael Niemeyer and Andreas Geiger. GIRAFFE: representing scenes as compositional generative neural feature fields. In *CVPR*, 2021.
- [41] Minghan Qin, Wanhua Li, Jiawei Zhou, Haoqian Wang, and Hanspeter Pfister. Langsplat: 3d language gaussian splatting. In *CVPR*, 2024.
- [42] Alec Radford, Jong Wook Kim, Chris Hallacy, Aditya Ramesh, Gabriel Goh, Sandhini Agarwal, Girish Sastry, Amanda Askell, Pamela Mishkin, Jack Clark, Gretchen Krueger, and Ilya Sutskever. Learning transferable visual models from natural language supervision. In *ICML*, 2021.
- [43] Zhongzheng Ren, Aseem Agarwala, Bryan C. Russell, Alexander G. Schwing, and Oliver Wang. Neural volumetric object selection. In *CVPR*, 2022.
- [44] Carsten Rother, Vladimir Kolmogorov, and Andrew Blake. "grabcut": interactive foreground extraction using iterated graph cuts. *ACM TOG*, 2004.
- [45] Konstantin Sofiiuk, Ilya A Petrov, and Anton Konushin. Reviving iterative training with mask guidance for interactive segmentation. In *ICIP*, 2022.
- [46] Karl Stelzner, Kristian Kersting, and Adam R Kosiorek. Decomposing 3d scenes into objects via unsupervised volume segmentation. *arXiv preprint arXiv:2104.01148*, 2021.
- [47] Julian Straub, Thomas Whelan, Lingni Ma, Yufan Chen, Erik Wijmans, Simon Green, Jakob J Engel, Raul Mur-Artal, Carl Ren, Shobhit Verma, et al. The replica dataset: A digital replica of indoor spaces. *arXiv preprint arXiv:1906.05797*, 2019.
- [48] Cheng Sun, Min Sun, and Hwann-Tzong Chen. Direct voxel grid optimization: Super-fast convergence for radiance fields reconstruction. In *CVPR*, 2022.
- [49] Vadim Tschernezki, Iro Laina, Diane Larlus, and Andrea Vedaldi. Neural feature fusion fields: 3d distillation of self-supervised 2d image representations. In *3DV*, 2022.
- [50] Suhani Vora, Noha Radwan, Klaus Greff, Henning Meyer, Kyle Genova, Mehdi SM Sajjadi, Etienne Pot, Andrea Tagliasacchi, and Daniel Duckworth. Nesf: Neural semantic fields for generalizable semantic segmentation of 3d scenes. *TMLR*, 2022.
- [51] Suttisak Wizatwongsa, Pakkapon Phongthawee, Jiraphon Yenphraphai, and Supasorn Suwajanakorn. Nex: Real-time view synthesis with neural basis expansion. In *CVPR*, 2021.
- [52] Mingqiao Ye, Martin Danelljan, Fisher Yu, and Lei Ke. Gaussian grouping: Segment and edit anything in 3d scenes. *arXiv preprint arXiv:2312.00732*, 2023.
- [53] Haiyang Ying, Yixuan Yin, Jinzhi Zhang, Fan Wang, Tao Yu, Ruqi Huang, and Lu Fang. Omniseg3d: Omniversal 3d segmentation via hierarchical contrastive learning. In *CVPR*, 2024.
- [54] Hong-Xing Yu, Leonidas J. Guibas, and Jiajun Wu. Unsupervised discovery of object radiance fields. In *ICLR*, 2022.
- [55] Shuaifeng Zhi, Tristan Laidlow, Stefan Leutenegger, and Andrew J. Davison. In-place scene labelling and understanding with implicit scene representation. In *ICCV*, 2021.
- [56] Xueyan Zou, Jianwei Yang, Hao Zhang, Feng Li, Linjie Li, Jianfeng Wang, Lijuan Wang, Jianfeng Gao, and Yong Jae Lee. Segment everything everywhere all at once. In *NeurIPS*, 2023.

A Appendix

In this appendix we provide the concrete training strategy of SAGA and implementation details. Then, we provide details about the open-vocabulary segmentation ability of SAGA and analyze its limitation. We also provide more visualization results to show the effectiveness of SAGA intuitively.

A.1 Detailed Additional Training Strategy

During the contrastive-based learning, an unavoidable problem is the data imbalance. In SAGA, the data imbalance is reflected in the following three aspects: 1) Scale-sensitivity imbalance. The majority of pixel pairs exhibit insensitivity to changes in scale. In other words, during a training iteration, most pixel pairs maintain their positive or negative classification regardless of scale variations. This makes the scale gate collapse to constant output; 2) Positive-negative samples imbalance. The majority of pixel pairs shows negative correspondence, resulting in segmentation features degradation; 3) Target-size imbalance. Large targets that occupy more pixels in images have more effect on the optimization, which leads to bad performance of segmenting small targets.

We use a resampling strategy to tackle the scale-sensitivity imbalance and positive-negative samples imbalance. Then, we adopt a pixel-wise re-weighting strategy to tackle the target-size imbalance.

Resampling In each iteration of training, we randomly select N_s scales and N_p pixels within an image and form $N_p \times N_p$ pixel pairs. Calculating the mask correspondence for these pixel pairs at every sampled scale results in a scale-conditioned correspondence matrix $\mathbf{R} \in \{0, 1\}^{N_s N_p N_p}$. We split the pixel pairs into three sets according to \mathbf{R} : 1) Inconsistent set: $\mathcal{Q}^{\text{in}} = \{(\mathbf{p}_1, \mathbf{p}_2) \mid \exists s_1, s_2, \mathbf{R}(s_1, \mathbf{p}_1, \mathbf{p}_2) \neq \mathbf{R}(s_2, \mathbf{p}_1, \mathbf{p}_2)\}$; 2) Consistent positive set: $\mathcal{Q}^{\text{pos}} = \{(\mathbf{p}_1, \mathbf{p}_2) \mid \forall s, \mathbf{R}(s, \mathbf{p}_1, \mathbf{p}_2) = 1\}$; 3) Consistent negative set: $\mathcal{Q}^{\text{neg}} = \{(\mathbf{p}_1, \mathbf{p}_2) \mid \forall s, \mathbf{R}(s, \mathbf{p}_1, \mathbf{p}_2) = 0\}$. During the loss calculation, all pixel pairs in \mathcal{Q}^{in} are involved. Then, we randomly select $\frac{|\mathcal{Q}^{\text{in}}|}{2}$ pixel pairs in both \mathcal{Q}^{pos} and \mathcal{Q}^{neg} respectively. To tackle the hard samples in training, we also add pixel pairs in \mathcal{Q}^{neg} which have feature correspondences larger than 0.5 and pixel pairs in \mathcal{Q}^{pos} which have feature correspondence smaller than 0.75 into loss calculation. This design not only ensures the sensitivity of the loss to scale changing but also keeps the balance of positive pairs and negative pairs. Let $\phi(\cdot)$ denote the sampling operation, after the resampling, we get three sets of pixel pairs, *i.e.*, $\mathcal{Q}^{\text{in}}, \phi(\mathcal{Q}^{\text{pos}}), \phi(\mathcal{Q}^{\text{neg}})$.

Re-weighting Considering two masks $\mathbf{M}_I^1, \mathbf{M}_I^2$ in \mathcal{M}_I , when uniformly sampling a pair of pixels, the probability that the pair is from $\mathbf{M}_I^1, \mathbf{M}_I^2$ is proportional to the product of the number of positive pixels of the two mask. This indicates that the optimization process is dominated by large masks. To re-weight the loss, we first calculate the mean mask size $m_{\mathbf{p}} = \frac{1}{|\mathcal{K}_{\mathbf{p}}|} \sum_{\mathbf{M} \in \mathcal{K}_{\mathbf{p}}} \sum_{i=1, j=1}^{H, W} \mathbf{M}(i, j)$ for each pixel, where $\mathcal{K}_{\mathbf{p}} = \{\mathbf{M} \mid \mathbf{M} \in \mathcal{M}_I, \mathbf{M}(\mathbf{p}) = 1\}$. For a pixel pair $(\mathbf{p}_1, \mathbf{p}_2)$, the loss weight is defined as $\omega(\mathbf{p}_1, \mathbf{p}_2) = \frac{1}{m_{\mathbf{p}_1} m_{\mathbf{p}_2}}$. All weights in a training iteration are then min-max normalized to the range $[1, 10]$ to ensure stable training.

With the resampling, re-weighting strategies, the overall loss function of SAGA is:

$$\begin{aligned} \mathcal{L} = & \frac{1}{|\mathcal{Q}^{\text{in}} \cup \phi(\mathcal{Q}^{\text{pos}})|} \sum_{(\mathbf{p}_1, \mathbf{p}_2) \in \mathcal{Q}^{\text{in}} \cup \phi(\mathcal{Q}^{\text{pos}})} \omega(\mathbf{p}_1, \mathbf{p}_2) \mathcal{L}_{\text{corr}}(\mathbf{p}_1, \mathbf{p}_2) + \\ & \frac{1}{|\mathcal{Q}^{\text{in}} \cup \phi(\mathcal{Q}^{\text{neg}})|} \sum_{(\mathbf{p}_1, \mathbf{p}_2) \in \mathcal{Q}^{\text{in}} \cup \phi(\mathcal{Q}^{\text{neg}})} \omega(\mathbf{p}_1, \mathbf{p}_2) \mathcal{L}_{\text{corr}}(\mathbf{p}_1, \mathbf{p}_2) + \\ & \frac{1}{HW} \sum_{\mathbf{p} \in \delta(\mathbf{I})} \mathcal{L}_{\text{norm}}(\mathbf{p}), \end{aligned} \quad (13)$$

where $\delta(\mathbf{I})$ denotes the set of pixels within the image \mathbf{I} .

A.2 Implementation Details

Across different scenes, SAGA maintains consistent hyper-parameters. The feature dimension D is set to 32. The K of KNN used in local feature smoothing is set to 16. Training of Gaussian affinity

features lasts for 10,000 iterations. In each iteration, we randomly sample eight different scales and 1,000 pixels (1000^2 pixel pairs) from the view for training. For different loss terms, we do not adjust any loss balance coefficients in experiments.

We extract the multi-view 2D masks with the SAM ViT-H model. For open-vocabulary segmentation, we use the OpenCLIP ViT-B/16 model. All training and inference is conducted on a single Nvidia RTX 3090 GPU.

Experiment Setting For the NVOS dataset, we randomly select positive and negative points from the scribbles on the reference view (provided by the NVOS dataset) to conduct promptable 3D segmentation. We then render the 3D segmentation result on the target view and evaluate the Intersection over Union (IoU) and pixel-wise accuracy against the provided ground truth. For each scene in the SPIn-NeRF dataset, we randomly select a subset of points within and outside the mask of the reference view as positive and negative prompts.

A.3 Vote-based Open-vocabulary Segmentation

To enable open-vocabulary 3D segmentation in radiance fields, previous studies [22, 30, 41, 2, 27] focus on aligning 3D language feature fields with the visual features extracted by CLIP [42] image encoder. Then 3D segmentation can be achieved by querying the language fields with the textual features. The process of training language feature field can be regarded as multi-view feature fusing, which, in essence, is a kind of vote mechanism. This motivate us to see whether SAGA can handle open-vocabulary segmentation with well-trained Gaussian affinity features at minimum modification.

Readers may wonder why we do not use grounding methods like Grounding-DINO [32] to locate the object and convert the location into point prompts, which can then be fed to SAGA. To answer this question, we emphasize the setting of open-vocabulary segmentation. We follow a stricter approach than previous studies, such as SA3D [7] and GaussianGrouping [52], which rely on Grounded-SAM to convert language prompts to visual prompts in a specific view. Specifying this view introduces additional prior knowledge. In SAGA, users do not need to query a specific view; all that is required for open-vocabulary segmentation is a text prompt. With this idea in mind, we introduce a vote-based open-vocabulary segmentation strategy.

Constructing Vote Graph by Clustering To cluster the multi-view masks, an intuitive way is to cluster their corresponding segmentation features. However, this is infeasible since the segmentation features in SAGA are scale-conditioned. Segmentation features for different masks are probably in different feature subspace. This drives us to find a kind of **global features** that is consistent across different scales for multi-view masks to enable global clustering.

We propose to use the segmented Gaussians as the global feature. First, we uniformly sample a set of anchor Gaussians \mathcal{A} from \mathcal{G} . Then, for a 2D mask $\mathbf{M} \in \mathcal{M}_I$ with scale s_M , we calculate its scale-conditioned feature as³:

$$\mathbf{f}_M = \frac{1}{\delta(\mathbf{M})} \sum_{\mathbf{p} \in \delta(\mathbf{M})} \mathbf{F}^{s_M}(\mathbf{p}). \quad (14)$$

Then we compute the similarities between \mathbf{f}_M and all anchor Gaussians in \mathcal{A} to get a segmentation result $\mathcal{A}_M = \{\mathbf{g} \mid \langle \mathbf{f}_g^{s_M}, \mathbf{f}_M \rangle > \tau, \mathbf{g} \in \mathcal{A}\}$. The distance between two masks $\mathbf{M}_1, \mathbf{M}_2$ is defined as their intersection over union of this 3D segmentation result, *i.e.*, $D(\mathbf{M}_1, \mathbf{M}_2) = \frac{|\mathcal{A}_{M_1} \cap \mathcal{A}_{M_2}|}{|\mathcal{A}_{M_1} \cup \mathcal{A}_{M_2}|}$. Then we perform HDBSCAN based on this distance map to cluster the 2D masks.

Vote-based Segmentation After clustering, we obtain a vote graph \mathcal{V} , where masks of the same 3D target (instance or part) are grouped together. In other words, each cluster centroid in \mathcal{V} represents a potential segmentation target in the 3D space.

For each 2D mask \mathbf{M}_I of image \mathbf{I} , we extract its visual feature by feeding the masked image $\mathbf{I} \odot \mathbf{M}_I$ to the CLIP visual encoder. During inference, given any text prompt, a relevancy score r_M is assigned

³For brevity, we continue to use $\delta(\cdot)$ to denote the set of positive pixels in 2D masks.

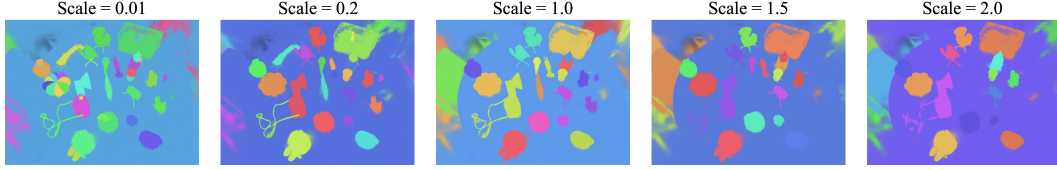


Figure 5: Adapting the scale gate mechanism with GARField achieves competitive results, demonstrating the potential of SAGA across different radiance fields.

to each mask \mathbf{M} by comparing the textual feature with the visual feature of the mask⁴. For a cluster centroid \mathbf{T} in \mathcal{V} , the relevancy scores of its corresponding 2D masks are aggregated to form its final relevancy score, *i.e.*,

$$r_{\mathbf{T}} = \frac{1}{|\mathcal{V}_{\mathbf{T}}|} \sum_{\mathbf{M} \in \mathcal{V}_{\mathbf{T}}} r_{\mathbf{M}}, \quad (15)$$

where $\mathcal{V}_{\mathbf{T}}$ is the set containing all 2D masks corresponding to the cluster centroid \mathbf{T} . For semantic segmentation in the 3D-OVS dataset, which provides a category list for each scene, the label of each cluster is assigned as the category with the highest relevancy score.

Limitation of SAGA in Open-vocabulary Segmentation The vote-based open-vocabulary segmentation strategy encounters difficulties in certain scenarios. For instance, when considering a bowl of noodles with an egg in it, SAGA ideally should distinguish between categories such as the egg, the egg with noodles (contents of the bowl), and the bowl with noodles and egg. However, because "egg" is included in masks at larger scales, CLIP often misclassifies larger objects as "egg." This issue is inherently rooted in the multi-granularity ambiguity in semantics. Addressing this problem is a promising research direction.

Another limitation is common among current CLIP-SAM based methods, such as LangSplat [41] and N2F2 [2]. Both SAGA and these methods first use SAM to segment the images and then use CLIP to attach semantics to these segments by segmenting the corresponding regions of the image and feeding them to CLIP. However, the effectiveness of the CLIP visual encoder also depends on context. For example, SAM sometimes segments the texture on a wall. Without seeing the entire wall, CLIP struggles to recognize it. This lack of context hinders the ability to ground the segments accurately. This is an important yet currently unexplored issue.

A.4 SAGA with Hybrid / Implicit Radiance Fields

Although SAGA is designed for segmentation in 3D-GS, its scale gate mechanism is not confined to a particular type of radiance field. We demonstrate this versatility by adapting SAGA to GARField, replacing the scale-conditioned affinity field with a scale-gated affinity field. As illustrated in Figure 5, the performance remains competitive.

A.5 More Qualitative Results

We present additional qualitative results in Figure 6 and Figure 7.

⁴We adopt the relevancy score introduced in LERF [22], which has been proven robust.

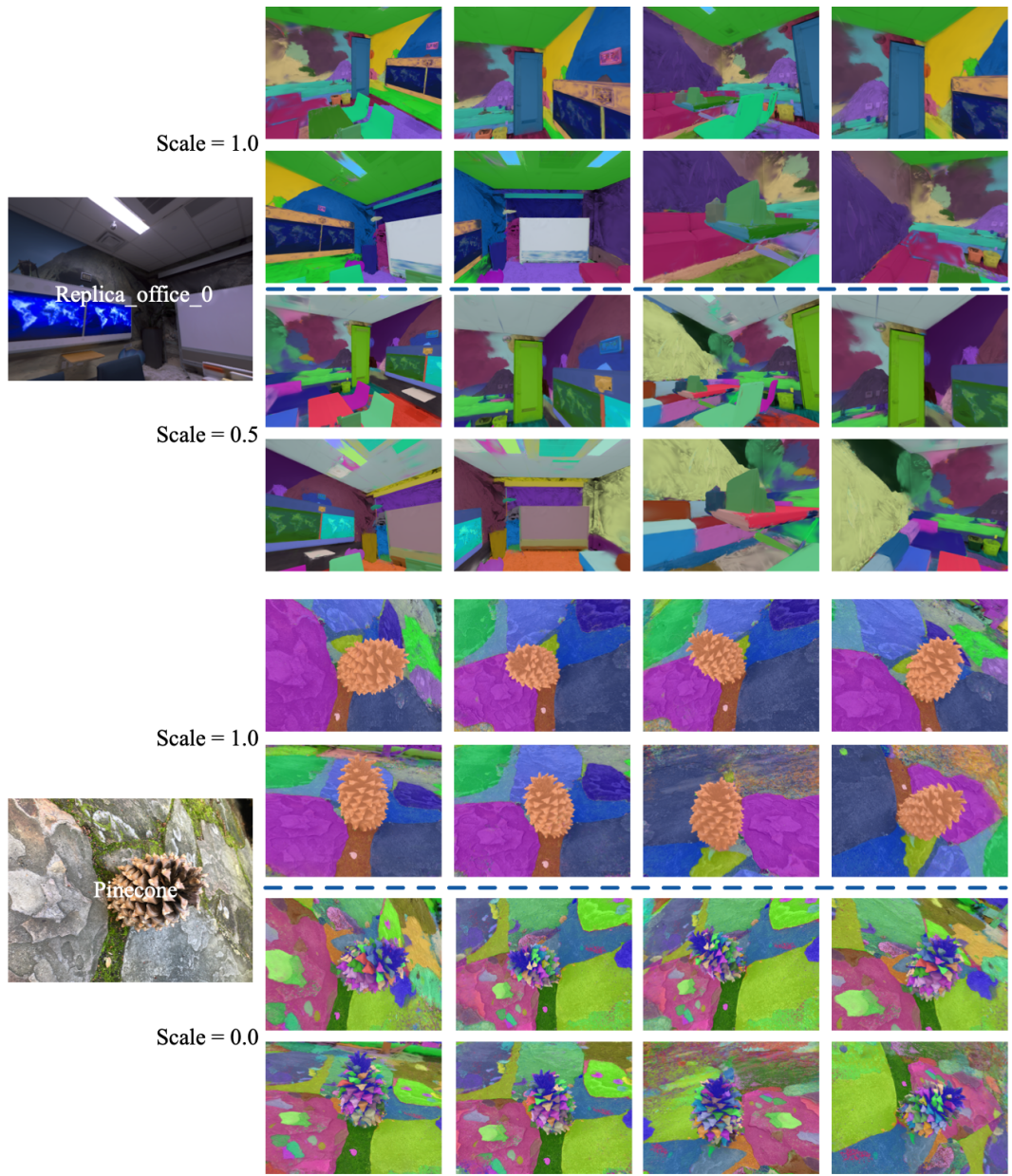


Figure 6: More qualitative results of SAGA.



Figure 7: More qualitative results of SAGA.